1. Large Helical Device (LHD) Project

The experiment with deuterium plasma started in 2017 in the Large Helical Device (LHD). The achievements in FY2020 include: (1) Establishment of a high-temperature plasma generation method, (2) Discovery of the positive side of turbulence, and (3) Observation of plasma-wave interaction.

(1) Establishment of a high-temperature plasma generation method

In the LHD deuterium plasma experiment in FY2020, we succeeded in generating plasmas with electron and ion temperatures of 100 million degrees. One hundred million degrees is one of the conditions for nuclear fusion and is an important milestone. Until now, plasmas with high ion temperatures have had low electron temperatures, but with this success, a method for producing plasmas that reach 100 million degrees has been established. With this success, the LHD research has entered a new stage.

(2) Discovery of the positive aspects of turbulence

In nuclear fusion, isotope mixture plasmas consisting of hydrogen isotopes deuterium and tritium are used. The LHD isotope mixture plasmas experiment using hydrogen and deuterium was conducted to simulate isotope mixture plasma. The hydrogen isotope mixing was observed for the first time in the world. It was found that turbulence, which has a large size, effectively mixes the hydrogen isotopes. The other finding is turbulence spreading. Turbulence does not occur in the absence of temperature or density gradients, but turbulence generated elsewhere can propagate to a region with a zero-gradient area, which is called turbulence spreading. The non-uniform flow in the plasma blocks the spreading turbulence. Furthermore, when this turbulence block is mitigated by MHD instability to enhance turbulent spreading in the plasma periphery, the heat load at the device's wall is reduced. The experiment revealed that turbulence, which has been emphasized as a negative aspect of nuclear fusion, has a positive aspect, and this achievement will become a basis for future fusion research.

(3) Observation of the interaction between plasma and waves

Two types of plasma instabilities occur when the pressure gradient becomes steep: those that appear slowly and persist and those that appear suddenly. Suddenly appearing instabilities are like earthquakes in that they can occur at any time, but we do not know when they will occur. For this sudden type, important experimental results were obtained to clarify the "trigger" and the "effect" on the plasma. Sudden instability is accompanied by the generation of waves like the tremors of an earthquake. The plasma generates these waves, but it was found that the impurities in the plasma absorb the waves and distort the velocity profile function. This interaction between plasma and waves is called "Landau damping," which the former Soviet physicist Landau proposed in 1946. Landau damping is one of the most significant discoveries in plasma physics, and the fact that this phenomenon was observed in the LHD plasma experiment is of great academic significance.

(K. Ida)

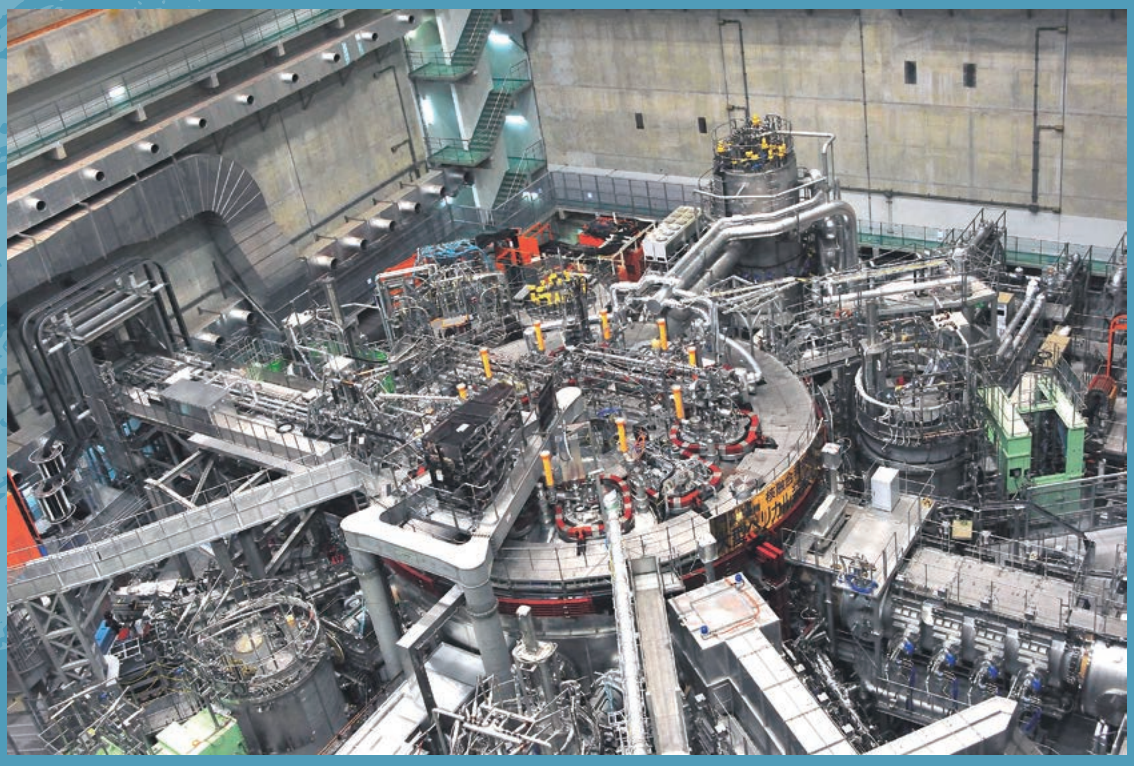

High Performance

Highlight

Extension of high-performance plasma operational regime

In the Large Helical Device (LHD), a deuterium (D) experiment was initiated in March 2017. To seek higher performance plasmas and to study the mechanism of the increased performance by isotope effect are the important purposes of the D experiments. In the FY2020 experimental campaign, we focused on the extension of the high temperature operational regime, of the high neutron emission ratio (S_n), and of the plasma stored energy (W_p).

Figure 1 shows the summary of the extension of the plasma performance [1]. We were able to successfully expand the high ion temperature (T_i) and the high electron temperature (T_e) regime due to the optimized heating combination of a neutral beam injection (NBI) and an electron cyclotron resonance heating (ECRH). Representative achievements are (1) T_{i0} = 10 keV with T_{e0} = 8.1 keV, and (2) both T_{i0} and T_{e0} = 8.7 keV (100 million degree). We renewed the S_n record of D pellet discharge as 4.1×10^{15} n/s from 3.3×10^{15} n/s using NB, ECH, and ICH. The experiments were conducted in the inward-shifted configuration of the R_{ax} = 3.55 m, where the EP confinement is better. The NB#1 and HAS were half and the new gyrotron was on low power operation. Thus, higher S_n is expected in the next campaign with heating operation in perfect condition. We also achieved a new record of W_p as 2.1 MJ with all NBs, ECH, and ICH. Under the n-NBI dominant condition, the achievable W_p is maximum at R_{ax} ~3.6 m, where the plasma volume is the maximum and is consistent with previous experiments. On the other hand, the achievable W_p increased as R_{ax} shifted inward under the p-NBI dominant, implying a better confinement of perpendicular beam components. In the R_{ax} = 3.75 m and 3.9 m, the SDC discharges were observed both for the H and the D pellet operation.

(H. Takahashi, K. Ogawa, R. Sakamoto)

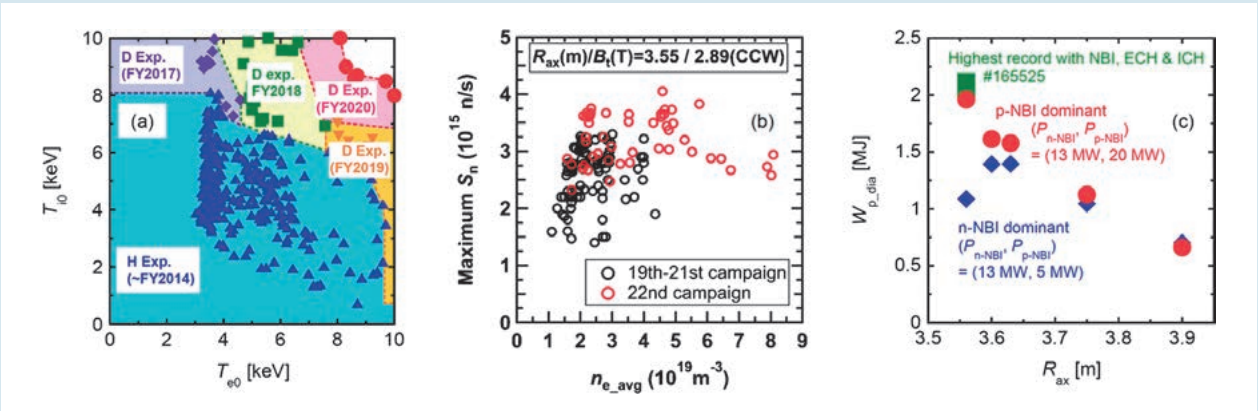

Fig. 1 (a) The operational map of high temperature plasmas, (b) the dependence of the S_n on the averaged n_e, and (c) the configuration dependence of the W_p [1].

Effect of an electron heating on high Ti operations

In the D experiments in the LHD, the simultaneous high T_i and high T_e regime has been successfully extended mainly due to the suppression of the EIC modes and control of the T_e/T_i value [2]. The EIC is triggered by helically trapped ions at a lower order magnetic resonant surface and the EIC causes loss of high energy ions, leading to the decrease in T_i [3]. The mode width of the EIC depends on $T_e^{-1/2}$ thus the increase in T_e at the resonant surface is expected to be effective to suppress the EIC. Figure 2 shows the comparison of the time evolution of (a) the heating power, (b) the line-averaged-electron density n_{e_fir}, (c) the poloidal magnetic fluctuation amplitude b_θ, (d) the neutron emission rate S_n, (e) the T_{i0} without and with 0.95-MW ECRH superposition. The bursty increase of b_θ and the synchronized drop in the S_n correspond to the EIC occurrence and the loss of the high energy ions, respectively. Due to the ECRH the EIC was clearly suppressed. Then the S_n, which is reflected the amount of the confined high energy ions, increased and this contributed to realizing the higher T_{i0}.

Although the ECRH is effective in mitigating the EIC, the increase in T_e/T_i causes a destabilization of the ITG mode [4], leading to a degradation of the ion thermal confinement. Figure 3 shows the ECRH power dependence of (a) number of the EIC bursts during the high T_i discharges and (b) the T_{i0} and the T_{e0}. The plasmas were produced using high power NBIs with the n_{e_fir} ~1×10^{19} m^{-3} and the ECRH was superposed on the high T_i plasmas. The numbers of the EIC burst clearly decreased with increase in the superposed ECRH power. The T_i value increased in low power ECRH conditions due to the EIC suppression. On the other hand, the T_i decreased in higher ECRH power superposition. This is due to the degradation of the ion thermal confinement in the plasma core region, due to the increase in the T_e/T_i.

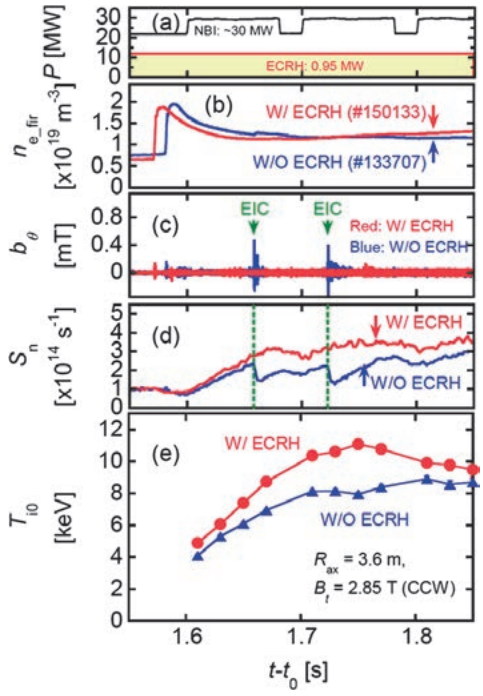

Fig. 2 The time evolution of (a) the heating power, (b) the n_{e_fir}, (c) the b_θ, (d) the S_n, and (e) the T_{i0} without and with ECRH superposition.

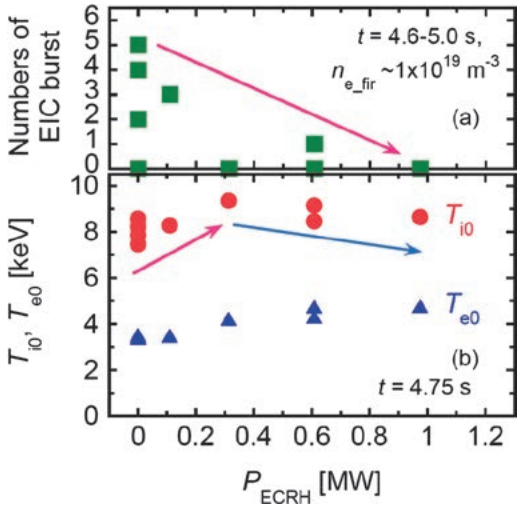

Fig. 3 The ECRH power dependence of (a) the numbers of the EIC burst during the high T_i discharges and (b) the T_{i0} and the T_{e0}.

Figure 4 shows the dependence of the normalized scale length of T_i on the T_e/T_i at the effective minor radius of r_{eff} = 0.1 m. These data were obtained in the high T_i operation with the superposed on-axis ECRH power from 0 to 5.4 MW. A significant degradation of the R/L_{Ti} was observed both in the H and D plasmas when the T_e/T_i exceeded ~0.7. These results show that not only the mitigation of EIC by ECRH but the control of T_e/T_i in the moderate range is important for realizing high T_i and high T_e simultaneously.

(H. Takahashi)

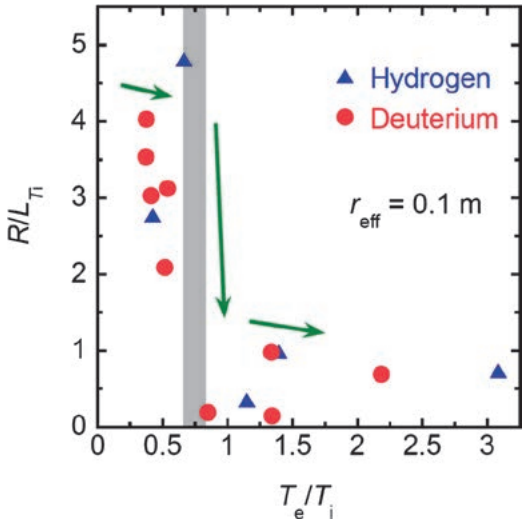

Fig. 4 The dependence of the R/L_{Ti} on the T_e/T_i at the effective minor radius of r_{eff} = 0.1 m.

Extension of the high total neutron emission rate of steady-state deuterium discharge guided by a data-driven approach.

One of the direct parameters for showing the path to a fusion reactor is fusion output which is connected to electrical power generation. In previous deuterium LHD campaigns, the total neutron emission rate (S_n) dependence on the electron density was surveyed in wide experimental conditions, i.e., the toroidal magnetic field strength (B_t) and the magnetic axis position (R_{ax}). It was reported that the relatively high S_n ~3.1×10^{15} n/s was achieved in a steady-state deuterium gas puff discharge at the so-called inward shifted and subcooled condition B_t = 2.89 T and R_{ax} = 3.55 m [5,6]. In the 22nd LHD campaign, we newly employed the data-driven approach, which is a complementary technique of physics-based methodology with no physics concerns, to guide a high S_n discharge scenario. The regression analysis, using externally controllable parameters, e.g., electron density and heating power, obtained in the previous campaign was executed to inspect the parameter importance toward high S_n achievement. In this analysis, data points fulfilling the following conditions were selected. (1) B_t = 2.89 T, and R_{ax} = 3.55 m. (2) A deuterium gas puff discharge without deuterium pellets. (3) All deuterium NBs were injected. (4) Deuterium dominant plasma with line-averaged electron density n_{e_avg} of 1×10^{19} m^{-3}. (5) The plasma initiation phase is excluded. The regression analysis is performed using only controllable parameters from the outside, e.g., n_{e_avg} [10^{19} m^{-3}], injection power of negative-ion based NB $P_{N\text{-}NB}$ [MW], injection power of positive-ion based NB $P_{P\text{-}NB}$ [MW], and injection power of electron cyclotron heating P_{ECH} [MW]. The regression expression $S_n = 10^{14.25} \times n_{e\_avg}^{0.52} \times P_{N\text{-}NB}^{0.69} \times P_{P\text{-}NB}^{0.37}$ is obtained [7]. Note that P_{ECH} was excluded from this regression analysis because the importance of P_{ECH} was relatively low, compared with the other parameters. The experimental scenario for high S_n was decided based on the obtained regression expression.

Figure 5 represents the time evolution of steady-state discharge that we achieve the new S_n record [8]. In this discharge, $P_{N\text{-}NB}$, $P_{P\text{-}NB}$, P_{ECH}, and the injection power of ion cyclotron heating P_{ICH} were 6.9 MW, 19.3 MW, 4.3 MW, and 2.4 MW, respectively. Especially, $P_{N\text{-}NB}$ injection power increases by 0.9 MW more than the previ-

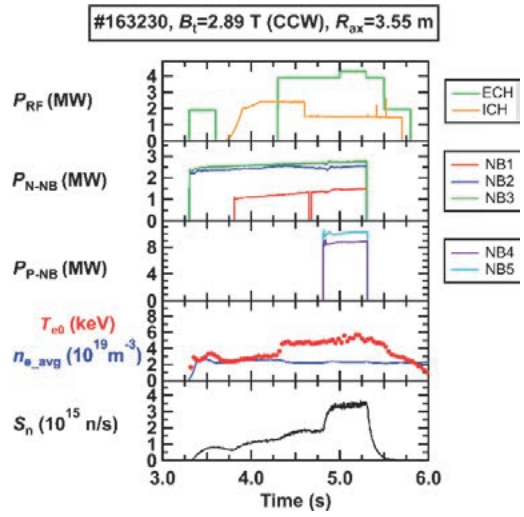

Fig. 5 Highest S_n steady-state discharges.

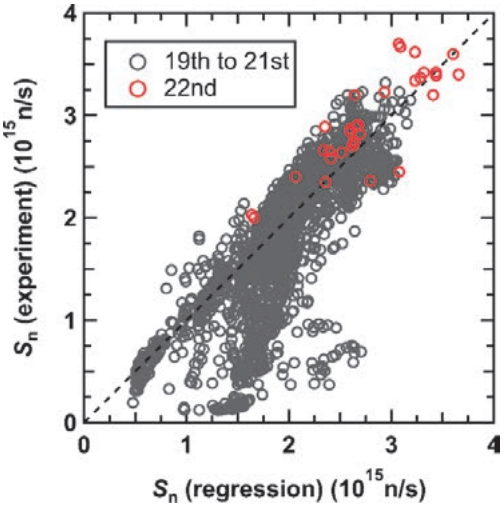

Fig. 6 Comparison of S_n measured in experiment and calculated by regression analysis in steady-state discharges.

ous high S_n discharge in steady-state conditions. The highest S_n of 3.7×10^{15} n/s in the steady-state discharge was successfully achieved in discharge number 163230 at $t = 5.236$ s. We have extended the S_n by approximately 20% from the previous campaigns. The relation between experimentally obtained S_n in s steady-state discharge and S_n, calculated by the regression expression, is indicated in Fig. 6. Here, the data taken through the 22nd campaign, indicated by the open red circles, are overplotted with the data taken through previous campaigns represented by the open gray circles. Although the regression expression is only applicable in s range of utilized databases, it is found that this regression approach can be used for showing a guideline to extend the parameter range slightly beyond the employed database.

(K. Ogawa)

[1] H. Takahashi *et al.*, presented in the 4th LHD Workshop, Toki, #2 (2021).
[2] H. Takahashi *et al.*, proc. 28th IAEA Fusion Energy Conference (virtual), CN-781 (2021).
[3] K. Ogawa *et al.*, Nucl. Fusion **58**, 044001 (2018).
[4] M. Nakata *et al.*, Plasma Phys. Control. Fusion **58**, 074008 (2016).
[5] M. Isobe *et al.*, Nucl. Fusion Nuclear Fusion **58**, 082004 (2018).
[6] K. Ogawa *et al.*, Nucl. Fusion **59**, 076017 (2019).
[7] K. Ogawa *et al.*, Plasma Fusion Res. **15**, 1202087 (2020).
[8] K. Ogawa *et al.*, Fusion Eng. Des. **167**, 112367 (2021).

Transport and Confinement

Highlight

Progress in the development of turbulence diagnostics

To improve our understanding of the effects of turbulent transport on toroidal plasma confinement, we are studying the interaction of turbulence on various scales at the LHD. Mixed micro-scale turbulence phenomena, which include both the ion and the electron scale turbulences, is of especial interest in the high temperature plasma confinement study at present, and there are many theoretical studies. The LHD already has several ion-scale turbulence diagnostics, such as CO2 laser used 2D phase constant imaging (PCI), microwave Doppler reflectometer/backscattering (DBS), and beam emission spectroscopy (BES). Recently, a 90 GHz W-band millimeter-wave back-scattering system [1] was designed and installed for measuring the electron scale turbulence such as the electron temperature gradient (ETG) driven mode which has a high wavenumber ($k_\perp \rho_s \sim 40$ and $k_\perp \sim 40\,\mathrm{cm}^{-1}$). Figure 1 shows the cross-section of the observation line of sight of the back-scattering system. In order to achieve both high spatial resolution and spatial scanning, a metallic lens antenna was applied as an in-vessel focusing antenna.

Simultaneous measurements of each ion scale turbulence and electron scale turbulence have been obtained. As an example, a comparison of the turbulence intensities of different hydrogen isotopes, hydrogen (H) and deuterium (D), shows a seesaw behaviour as shown in Figure 2. The ion scale turbulence decreases more in the case of D than H, while the electronic scale turbulence increases slightly in the case of D. These results are qualitatively consistent with the predictions of the gyrokinetic simulation (GKV code) calculation [2], and provide a basis for discussion of the future importance of comparing the results of such multi-scale turbulence experiments and theoretical simulations.

[1] T. Tokuzawa *et al.*, Rev. Sci. Instrum. **92**, 043536 (2021).
[2] K. Tanaka *et al.*, Plasma Phys. Control. Fusion **62**, 024006 (2020).

(T. Tokuzawa)

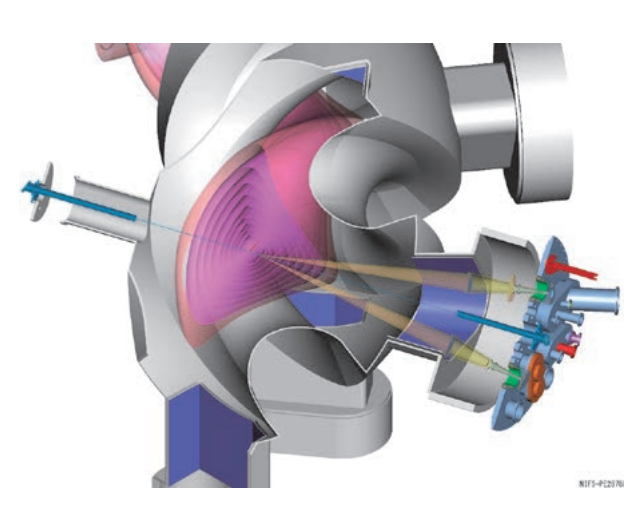

Fig. 1 In-vessel antenna pair for the back-scattering system. The millimeter wave beams of the launcher and receiver are represented by yellow triangles. [1]

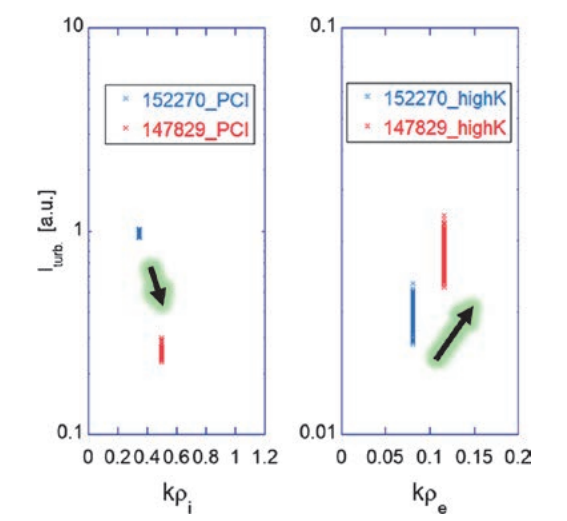

Fig. 2 Comparison of turbulence intensity in hydrogen (blue crosses) and deuterium (red crosses) plasmas. Ion scale turbulence (left) and electron scale turbulence (right).

Observation of heat flux driven by turbulence pulse during minor collapse of electron internal transport barrier [3]

Minor collapses of the electron internal transport barrier (e-ITB) are repeatedly observed by controlling the rotation transform profile with the electron cyclotron current drive (ECCD) and the neutral beam current drive (NBCD) to form a magnetic island in the central region of the plasma, which increases the pressure gradient in the e-ITB region. Figure 3 shows the time evolution of the electron temperature profile and the electron temperature gradient near the e-ITB foot, measured by a newly developed high time resolution (repetition rate: 20 kHz) Thomson scattering diagnostics. As shown in Fig. 3 (b), the pressure gradient near the e-ITB foot increases due to the formation of the magnetic island, and reaches a threshold value of about 12 keV/m. When the pressure gradient reaches this value, the e-ITB collapses. After the collapse, the temperature gradient increases again, leading to another subsequent collapse.

At the timing of the collapse of the e-ITB, the time evolution of the electron temperature, the electron scale turbulence, and the magnetic field fluctuation are investigated by an ECE measurement, a backscattering measurement, and a magnetic probe, respectively (Fig. 4). It is suggested that the formation of a magnetic island in the central region of the plasma causes a strong pressure gradient, which leads to MHD instability, and the resulting turbulent transport propagates the heat flux outward, causing minor collapses of the e-ITB. Since the electron-scale turbulence rises and falls in a very short time of about 300 μsec, it is considered to have a pulse shape with a spatial width of the line of sight. The electron-scale turbulence is scanned shot-by-shot at the spatial position to investigate the radial propagation speed. The turbulence pulse propagates outward at a speed of about 10 km/s from the core (r_{eff}/a_{99}~0.1) to the edge region (r_{eff}/a_{99}~1.0), while the thermal pulse propagates at a speed of 1.5 km/s.

In this research, strong pressure gradients are generated by forming magnetic islands inside the e-ITB plasma, which induce instabilities and generate observable turbulence that is larger than the background turbulence. Such a large turbulence enables us to observe the propagation of the turbulence pulse. This method can artificially induce turbulence spreading and avalanche, caused by the collapse of e-ITB, and is beneficial for understanding the physics of avalanche and turbulence spreading.

[3] N. Kenmochi *et al.*, submitted to Communications Physics.

(N. Kenmochi)

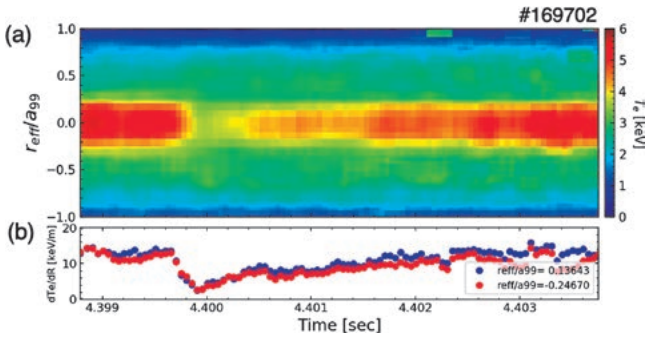

Fig. 3 The time evolution of (a) the electron temperature profile and (b) the electron temperature gradient near the e-ITB foot observed by the newly developed high time resolution (repetition rate: 20 kHz) Thomson scattering measurement.

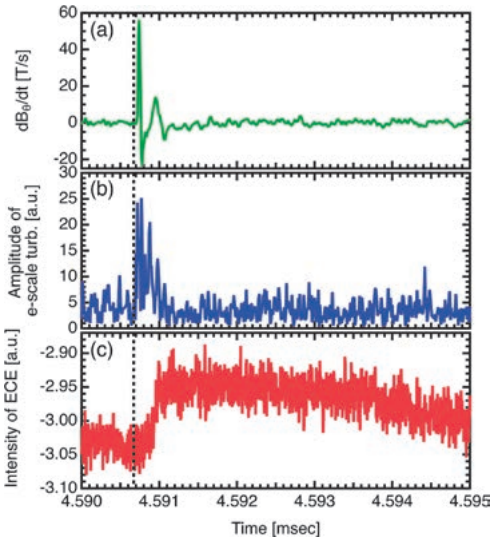

Fig. 4 The time evolution of (a) magnetic fluctuation, (b) electron scale turbulence, and (c) electron temperature measured by magnetic probe, W-band back scattering measurement, and ECE measurement, respectively.

Development of fast charge exchange spectroscopy system with fast camera

As the energetic ion driven mode and non-local transport and hysteresis phenomena have been observed in the plasma, the velocity distribution of ions and electrons have been a target of study to understand these behaviors. In the LHD, the energetic ion driven resistive interchange (EIC) mode, a rotating bursting m/n = 1/1 tearing parity mode, which resonates with the precession motion of helically trapped energetic ions, has been observed during the heating by neutral ben injection with positive ion source (p-NBI).

The charge exchange system with a high sampling frequency (10 kHz) has been developed to observe the time change of the velocity distributions of carbon ion on the various plasma behaviors. Figure 5 shows the components of the spectrometer system. The fast camera (FASTCAM Nova PHOTRON LIMITED.) and image intensifier (C10880 **Hamamatsu** Photonics K.K.) are used as the detector of the spectra image instead of the CCD camera for the high sampling frequency. A bundle consisting of 200 optical fibers (400 um core), arranged in four slits of 50 fibers each, with smile curve correction, is used for the incident side. The 50 fibers are binned in a vertical direction to increase the signal light coming from the plasma and the system can be observed from four positions in space. The pixel size of the fast camera is 20 um, but since the image intensifier shrinks the image, the effective pixel size is 29 um. The inverse dispersion is 0.724 nm/mm, and the instrument width (FWHM) is 0.471 mm. The tangential lines of sight on the 9O port are used for this measurement because the lines of sight have a lot of channels (15 lines of 104 horizontal channels each) with a 1 cm pitch. The emission from the area of 14 cm vertically times 4 cm radially, is collected with the 50 channels of the slit in the incident bundle.

Figure 6 (a) shows the time traces of the Wp and RF probe signal in the discharge in which are observed MHD burst events. The stored energy Wp is dropped down associated with the spikes in the RF probe signal, which indicates the activities of the energetic ions. The magnetic axis position R_{ax}, toroidal magnetic field B_T, canceling ratio of the quadrupole component B_q, and pitch parameter are 3:6 m, –2.75 T, 100%, and 1.254, respectively. The electron density and temperature at the plasma center are 2.5×10^{19} m^{-3} and 1.3 keV, respectively. Figure 6 (b) shows the time change of the CVI (529.05 nm) spectra around R = 4.25 m, measured with the sampling frequency of 10 kHz. The CVI spectra were observed to spread only to the longer wavelengths when the event

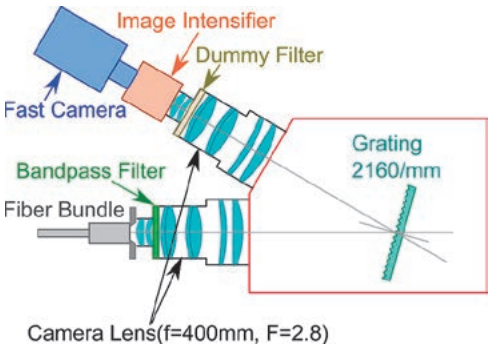

Fig. 5 Schematic view of the spectrometer for the fast charge exchange spectroscopy system.

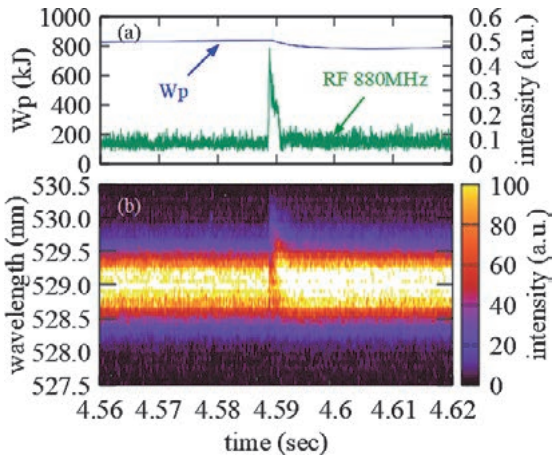

Fig. 6 (a) time trace of Wp and RF probe signal. (b) time change of CVI spectra around the MHD burst event (#164344).

happened and it recovered in a very short time. From the spectra obtained in this way with high time resolution, the distortion of the velocity distribution of ions from the Maxwell distribution when the event happened can be investigated using moment analysis.

(M. Yoshinuma, K. Ida, T. Kobayashi)

Study of ICRF minority hydrogen ion heating characteristics in deuterium plasma in the LHD

The characteristics of the ion cyclotron range of frequency (ICRF) minority ion heating with hydrogen minority and deuterium majority plasma were studied by an ICRF modulation injection experiment in the LHD. In recent experimental conditions with deuterium plasma, a significant increase of the neutron emission rate by ICRF second harmonic deuteron heating was not observed [4]. Therefore, in this study, the neutron emission rate is used to refer to the information regarding the thermal ion component. The experimental and simulation results of the heating efficiencies in the various minority hydrogen ion ratios are shown in Fig. 7 (a). The heating efficiencies of the HAS antenna and FAIT antenna were observed separately. The dashed lines are the results of the estimation of the total heating efficiency and that of the electron direct heating, using a simple-model simulation [5]. The experimental results showed good agreement with the simple-model simulation of the ICRF wave absorption. Fig. 7 (b) shows the simulation result of the spatial distribution of the absorbed power in the case of a minority hydrogen ratio of 2%. The strong absorption can be seen at around the region where the left-hand polarized electric field is locally. During these experiments, the accelerated minority hydrogen ions were observed by neutral particle analyzers (NPAs) [6]. As shown in Fig. 7 (c), the counting rates of the energetic particles were higher in the lines of sight of passing through the helical ripple than that of across the magnetic axis. The counting rate decreased as the minority hydrogen ion ratio increased. The dependence of the minority hydrogen ion ratio on the density of the energetic ions was consistent with the heating efficiencies experimentally observed and of simulation. The heating efficiency of the ICRF minority ion heating could be well explained by simple-model simulation in the LHD deuterium experiment.

[4] R. Seki *et al.*, 2020 *Plasma Fusion Res.* **15**, 1202088.
[5] K. Saito *et al.*, 2001 *Nucl. Fusion* **41**, 1021-1035.
[6] S. Kamio *et al.*, 2019 *JINST* **14**, C08002.

(S. Kamio)

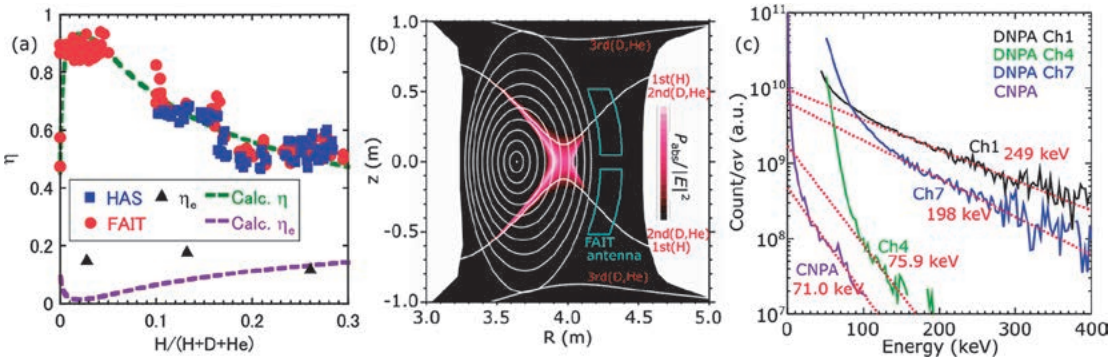

Fig. 7 (a) Experimental and simulation results of the heating efficiencies depending on the minority hydrogen ratio. (b) Spatial distribution of the absorbed power in the calculation in the case of the minority hydrogen ion ratio of 2%. (c) Energy distributions of the accelerated energetic particles observed by NPAs.

Edge/Divertor/Atomic and Molecular Processes

Highlight

Confinement mode transition during detached phase with RMP application in LHD

Compatibility of good core plasma performance with divertor heat load mitigation is mandatory for future reactors. In LHD, impact of the edge magnetic field structure on the core confinement and divertor detachment is being observed. The RMP (resonant magnetic perturbation) field (m/n = 1/1) application creates edge magnetic island. It has been found that the edge island has stabilizing effect on the detachment operation [1]. In the deuterium experiments with the RMP application, confinement mode improvement is observed [2]. Figure 1 shows time traces of plasma stored energy (Wp), divertor particle flux, magnetic probe signal, and pressure gradient profile. The detachment transition occurs at t = 3.95 sec as confirmed with the reduction of the divertor particle flux. At the same time, increase of Wp is observed together with formation of edge pressure gradient. In the latter phase of the detachment, further increase of Wp occurs spontaneously at t = 4.5 sec, where strong edge transport barrier (ETB) is formed as shown in the pressure gradient profile in Fig. 1 (d). The ELM like burst appears in the magnetic probe signal as well as in the divertor particle flux. The density fluctuation measured by the 2D phase contrast imaging decreases by an order of magnitude during the ETB formation. These are clear signature of the confinement mode transition as observed in the H-mode in tokamaks. It has been found that the ETB develops at the inner edge of the magnetic island created by the RMP. It is also found that the ETB is stronger in the deuterium plasmas than the hydrogen plasmas as shown in Fig. 2, where edge pressure profiles in detached phase are compared between deuterium and hydrogen plasmas. The results clearly show the importance of the edge magnetic field structure and isotope effect on the core confinement compatible with the diverter detachment for the heat load mitigation. The mechanism of the confinement mode transition is under investigation to extrapolate to a future reactor operation scenario.

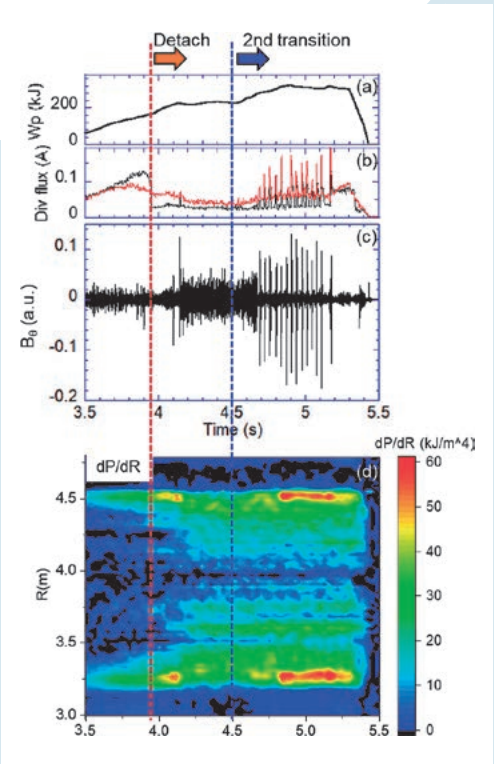

Fig. 1 Time traces of (a) plasma stored energy (Wp), divertor particle flux, (c) magnetic probe signal, (d) radial profile of pressure gradient, with RMP application in deuterium plasma.

[1] M. Kobayashi *et al.*, Nucl. Fusion **59**, 096009 (2019).
[2] M. Kobayashi *et al.*, IAEA FEC 2020, EX/2.

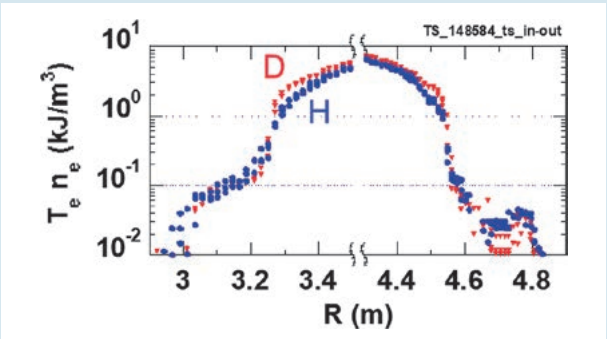

Fig. 2 Radial profile of pressure at the edge region during divertor detachment operation with RMP application. Red: deuterium, blue: hydrogen.

Impact of boron powder dropping on plasma operation

Impurity powder dropping (IPD) experiment has been conducted in the Large Helical Device (LHD) for a collaborative research between PPPL and NIFS to investigate the effects of the real-time wall conditioning on plasma and plasma-wall interactions [3–6]. Boron (B) powder was dropped from a top port (see the middle figure in Fig. 3) to high temperature plasmas with central electron temperature of several keV with a typical dropping rate of several tens of mg/s.

It has been observed that emission intensities of Hα and low-Z impurities decreases with the B powder dropping as shown in the left figure in Fig. 3. The figure which shows time evolutions of the emission intensities with and without the B dropping in two hydrogen discharges with the same line averaged density. The figure clearly shows that the real-time wall conditioning with the B powder dropping works effectively as expected.

The figure also shows that the emission intensity of Fe XVI decreases with B powder dropping. On the other hand, it has been observed that emission intensities of low charged Fe ions do not decrease with the B powder dropping (not shown in Fig. 3). This suggests that generation of Fe impurity does not change but transport changes with the B powder dropping.

Neutral pressure measured at an outer horizontal port also decreases with the B dropping suggesting wall pumping works during the dropping. The suppression of fuel recycling has been observed not only for hydrogen isotopes but also helium. It is well known that hydrogen isotopes are absorbed by a B film on plasma facing wall. In the case of the B dropping, absorption on the formed B film and co-deposition of fueled particles and B simultaneously work. As a result, it is possible that helium recycling is also suppressed by the co-deposition.

Another interesting effect of the B powder dropping has been observed in ion and electron temperatures as shown in the right figure in Fig. 3. Line averaged densities in the two discharges shown in the figure were the

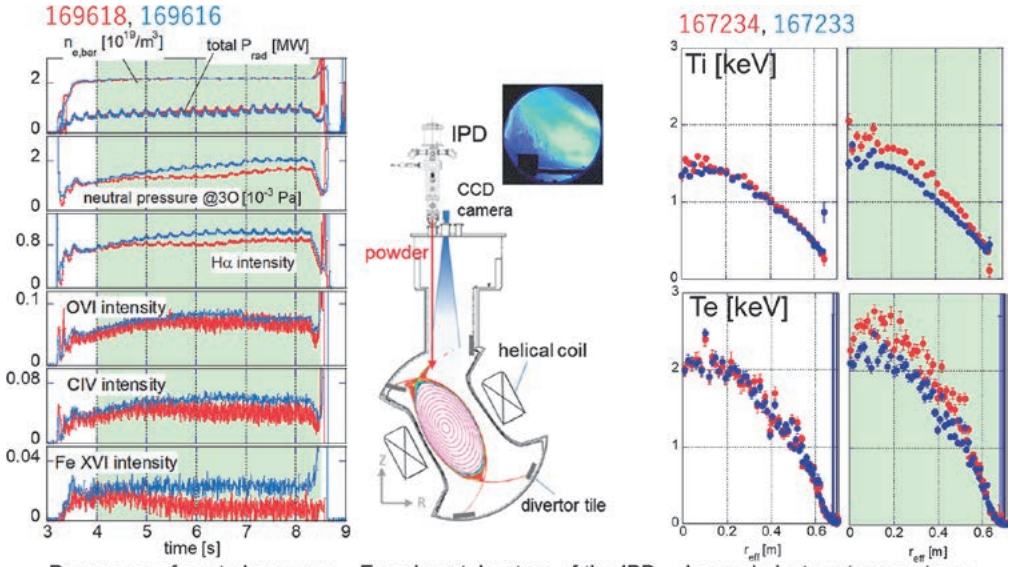

Decreases of neutral pressure and emission intensities of H alpha, OVI, CIV, Fe XVI during the B powder dropping

Experimental set-up of the IPD and a view of the CCD camera during B powder dropping

Ion and electron temperatures rises during the B powder dropping

Fig. 3 Effects of the B powder dropping on plasma operation. In all graphs, red and blue show data with and without the B powder dropping, respectively, and the terms of the B powder dropping are shown by the green hatched parts.

same. By the B powder dropping, both ion and electron temperature rises. This temperature rises have been observed not only in NBI heated plasmas but also an ECH and ICH plasma. A suppression of density fluctuation has been observed during the B powder dropping by the Phase Contrast Imaging (PCI) measurement, and that suggests a reduction of turbulent transport. That can cause the temperature rises.

[3] F. Nespoli *et al.*, Nucl. Mater. Energy **25**, 100842 (2020).
[4] F. Nespoli *et al.*, 28th IAEA Fusion Energy Conference.
[5] M. Shoji *et al.*, Nucl. Mater. Energy **25**, 100853 (2020).
[6] T. Oishi *et al.*, Plasma Sci. Tech. **23**, 084002 (2021).

(S. Masuzaki)

Polarization spectroscopy for the study of anisotropy in the electron velocity distribution function

The polarization of the Lyman-α line has been measured with an accuracy of 1%. The analysis of the polarization angle showed that the electron motion perpendicular to the magnetic field is more dominant than that parallel to the magnetic field, which supports our intuitive understanding of the electron confinement characteristics in the plasma edge region where the Lyman-α line emission mainly takes place.

The motion of electrons in the plasma can be divided into two components: the translation velocity in the magnetic field direction and the rotation velocity in the plane perpendicular to the magnetic field direction. Electrons with a large velocity component moving in the magnetic field direction will continue to move along the magnetic field lines, while particles with a large rotational velocity component will tend to be trapped in regions with low magnetic field strength when the magnetic field strength along the magnetic field lines has a modulation.

Electrons in the plasma edge, when flung out of the confinement region due to collisions with other particles, are guided along the magnetic field lines to the vessel wall and are lost, while electrons with a large rotational velocity component tend to stay in the plasma for the reasons mentioned above. It has been therefore pointed out that the directional distribution of electron motion outside the confinement region may be anisotropic. This anisotropy in electron motion affects the ionization rate of the atoms which influences the plasma production characteristics and is also thought to be involved in the formation of the electric field that plays an important role in determining the confinement performance of the plasma.

A possible clue for understanding the anisotropy of electron motion is the light emitted by atoms or ions in the plasma [7]. When an atom collides with an electron, it receives a portion of the electron's kinetic energy and is excited to a higher energy state. Since the excited states are unstable, it returns to its original low energy state after a short period of time (typically about a nanosecond), and the energy difference between the two states is emitted as a photon or a light.

The light is a kind of electromagnetic wave. Electromagnetic waves oscillate in a direction perpendicular to their direction of motion. The azimuthal angle of oscillation is arbitrary, and most of the light we see in our daily lives is a mixture of waves oscillating at various azimuthal angles to the same degree. However, there are some

cases where the intensity of the waves differs depending on the azimuth angle. Such light is called “polarized”.

The azimuthal angle of the light oscillation coming out of an atom colliding with an electron is affected by the direction of the colliding electron’s motion as shown in Fig. 4. We are studying the magnitude of the polarization of the light emitted by hydrogen atoms to determine the anisotropy of the electron motion in the plasma [8].

In LHD and other plasmas aimed at nuclear fusion, the expected polarization degree is so small that it is necessary to detect a difference in light intensity of about 1%. Based on the hints obtained in the joint research with the Solar observation group of the National Astronomical Observatory of Japan (NAOJ) [9], and after several years of development of measurement instruments, we finally succeeded in realizing high-precision polarization measurement at the LHD and actually detected the polarization as shown in Fig. 5. It was confirmed that the polarization of the emission lines occurs between the direction of the magnetic field and the direction perpendicular to it, and initial analysis showed that electrons moving perpendicular to the magnetic field, i.e., rotating electrons, have dominant distribution characteristics [10].

[7] T. Fujimoto and A. Iwamae, Eds., *Plasma Polarization Spectroscopy*, Springer, Berlin (2008).
[8] M. Goto and N. Ramaiya, *Symmetry* **13**, 297 (2021).
[9] R. Kano *et al.*, *ApJL* **839**, L10 (2017).
[10] N. Ramaiya *et al.*, *J. Quant. Spectrosc. Radiat. Transf.* **260**, 107430 (2020).

(M. Goto)

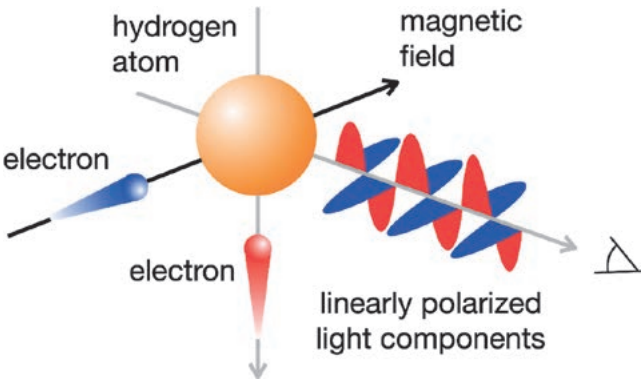

Fig. 4 Schematic diagram of the principle of polarization of light emitted by an atom in collision with an electron. Emission lines from collisions between blue and red electrons mainly correspond to the blue and red waves, respectively.

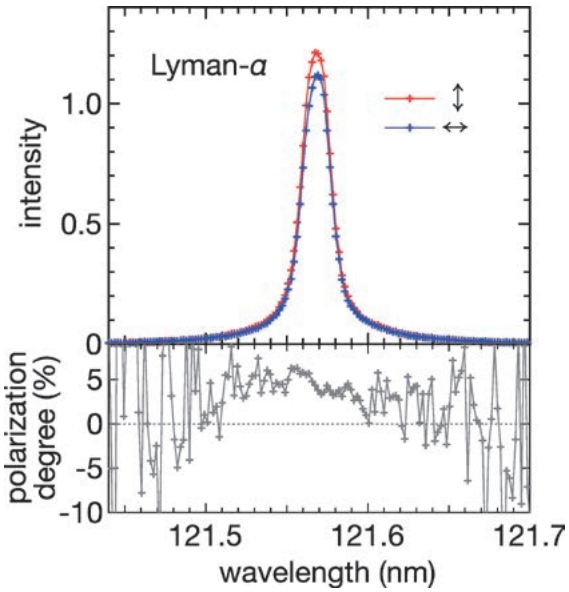

Fig. 5 An example of a polarized hydrogen atom emission spectrum observed at LHD. The upper figure shows the line profiles, with the red and blue lines showing the linearly polarized light components in the vertical and horizontal directions, respectively. The lower figure shows the difference between the red and blue lines in the upper figure divided by the sum of the two lines, which is called the polarization degree.

High-beta/MHD/Energetic Particles

Highlight

High-beta plasma production examined in Deuterium experiment

An aim of the LHD project is the realization of the reactor-relevant high-beta plasma, where the volume averaged beta, $\langle\beta\rangle$, is 5%, at B = 1~2 T. In the hydrogen experiment before the 19th campaign, the beta value achieved 3.4% and 4.1%, which are the quasi-steady state by the gas puffing and the transient by the pellet injection, respectively. However, in the deuterium experiment, due to the power degradation of the tangential NBI, the plasma start-up in the low field was impossible. For solving that problem, in the 21st campaign, only one tangential NBI keeps the hydrogen operation for expecting the high heating power. Then the high-beta production examined comparing with the hydrogen plasma.

Figure 1 shows the dependency of the achieved beta value on the line averaged density. The circle symbol indicates the quasi-steady state discharge by the gas puffing, and the triangle symbol indicates the transient discharge by the pellet injection. The color indicates the pre-set vacuum magnetic axis. For both quasi-steady state and transient discharges, the highest beta values were achieved at R_{ax} = 3.55 m. For discharges of the gas puffing, it seems the degradation due to the increased density, but for the pellet injection, there is no degradation by the increased density. The fine-tuning of the density is the next step.

(Y. Suzuki)

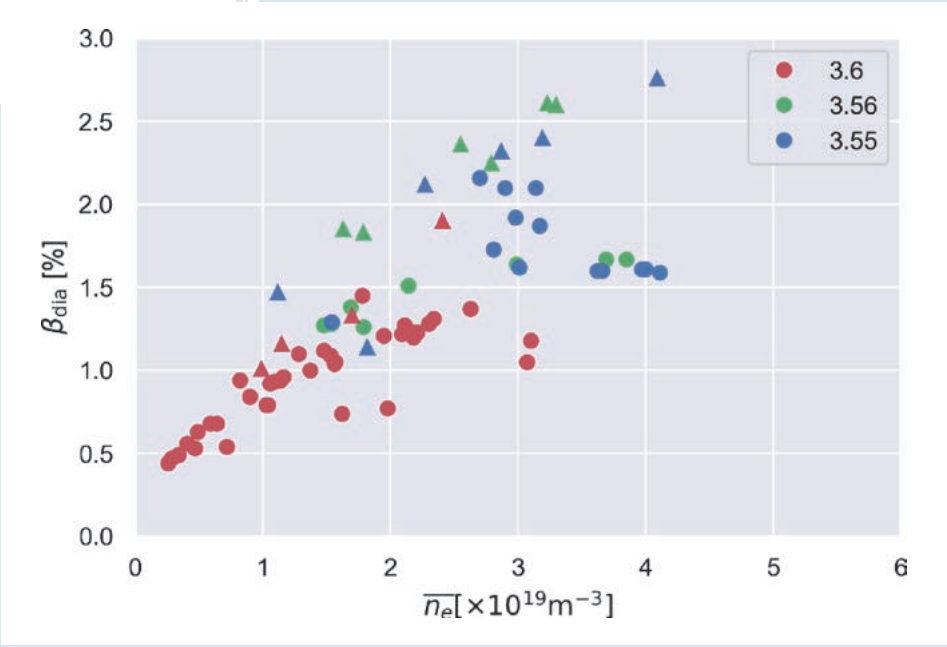

Fig. 1 the dependency of the achieved beta value on the line averaged density.

Energetic Particle Transport by Helically-trapped Energetic-ion-driven Resistive Interchange Mode in LHD

In high-ion temperature experiment performed in relatively low-density plasma with intense positive-ion-source based perpendicular neutral beam injections (P-NBI) in the Large Helical Device (LHD), the helically-trapped energetic-ion-driven resistive interchange mode (EIC) is often observed [1,2] and limits sustainment of the high-ion-temperature state [3]. To sustain the high-ion-temperature state for a longer period, a study of energetic ion transport due to EIC was performed using neutron diagnostics in LHD [4].

We used two vertical neutron cameras (VNCs) to measure the time evolution of the neutron profile. VNC1 [5] characterized by a high spatial resolution based on stilbene fast-neutron detector and VNC2 characterized by high detection efficiency based on EJ410 fast-neutron scintillator were installed under the floor concrete of the torus hall. VNC1 and VNC2 were installed in the vertical elongated poloidal cross section and the diagonal poloidal cross section, respectively. Figure 2 shows the typical density profile of helically-trapped beam ion created by P-NB injection in relatively low-density plasma calculated by MORH code [6] with sightlines of VNCs.

Figure 3 shows line-integrated neutron profiles measured by VNC1 and VNC2 before and after the EIC burst.

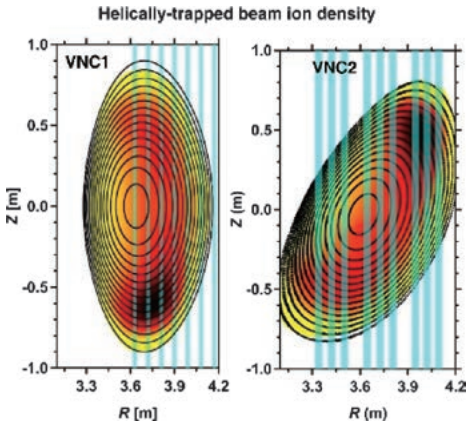

Fig. 2 Helically trapped beam ion density created by P-NB injection and sight lines of VNCs.

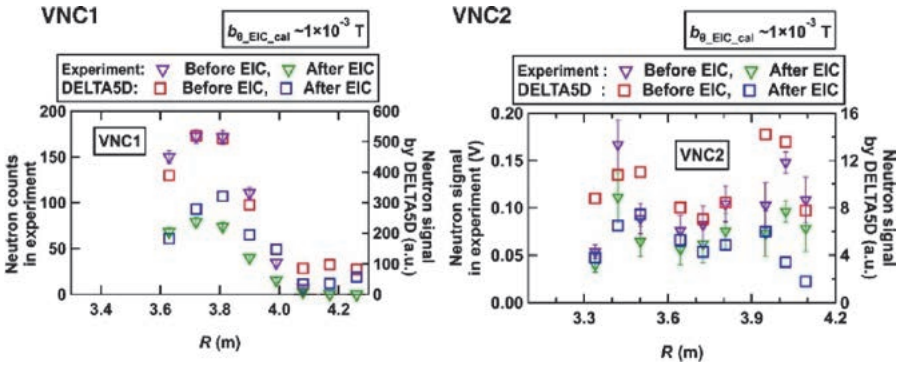

Fig. 3 Line-integrated neutron profile before and after the EIC burst.

Here, the neutron counts measured by VNC1 at a time interval of 20 ms and the averaged signals over 20 ms measured by VNC2 are plotted. These results showed that the neutron profiles were substantially changed due to the EIC burst. Guiding-center orbit-following simulations, including EIC fluctuations, were performed to understand the helically-trapped beam ion transport due to EIC. A comparison of the line-integrated neutron profile before and after the EIC burst measured in the experiment and obtained by the numerical simulation is shown in Fig. 3. The neutron profile for VNC1 shows a single peak appeared at R of approximately 3.75 m, which is nearly equal to the peak position measured in the experiment. The neutron counts for VNC1 at the central channel (R from 3.6 m to 3.9 m) becomes almost one-half after the EIC burst, as measured in the experiment. Although there are relatively wide peaks for line-integrated neutron profile for VNC2 compared with the experiment, the neutron signal shows two peaks in numerical calculation. A decrease in the neutron signal due to the EIC burst at two peaks corresponding to helical ripple valley is reproduced.

[1] Du X. D. *et al.*, 2015 Phys. Rev. Lett. **114**, 155003.
[2] Du X. D. *et al.*, 2015 Nucl. Fusion **56**, 016002.
[3] Takahashi H. *et al.*, 2018 Nucl. Fusion **58**, 106028.
[4] Isobe M. *et al.*, 2018 IEEE Trans. Plasma Sci. **46**, 2050.
[5] Ogawa K. *et al.*, 2018 Rev. Sci. Instrum. **89**, 113509.
[6] Seki R. *et al.*, 2015 Plasma Fusion Res. **10**, 1402077.

(K. Ogawa)

Observation of the Transported Particles Using an Upgraded Neutral Particle Analyzer during TAE Burst in the Large Helical Device

The bursting toroidal Alfvèn eigenmodes (TAEs) [1] are often observed in relatively low magnetic field experiments in the Large Helical Device (LHD). In previous studies, by measuring the transported neutral particles by the TAE burst using the E-parallel-B type neutral particle analyzer (E‖B-NPA) [2] and using the lost ion using scintillator-based fast-ion loss detector (FILD), the existence of the hole-clump pairs was suggested in real space [3–5]. To measure the time evolution of the energetic particles transported by TAE bursts in more detail, the E‖B-NPA was upgraded. The time duration of the observed single TAE burst is approximately 0.5 ms with the frequency chirping down. Therefore, the measurement time resolution is important for measuring the detailed structure of the transported energetic particles during the TAE burst. The measurement electronic circuits of the E‖B-NPA were updated, and the time resolution was improved up to 100 kilo samples per second [6].

During the tangential neutral beam (t-NB) #1 injection in the magnetic field at the magnetic axis is 0.6 T, TAE bursts were observed by the Mirnov coils and the E‖B-NPA. Figure 4 shows the (a) signal of the Mirnov coil, (b) the spectrogram of the magnetic fluctuations, and (c) the energy spectrum of the particle flux Γ observed by E‖B-NPA. The TAE bursts were observed with the time intervals of approximately 10 ms. During and after the TAE bursts, the transported particles were observed by E‖B-NPA. Figure 5 shows the result of the conditional averaging technique for the amplitude of the magnetic fluctuation and the changing of the observed particle flux $\Delta\Gamma$ measured by E‖B-NPA with using 72 TAE bursts. The peak amplitude of the magnetic fluctuation of 70 kHz is set to 2.0 ms. By the conditional averaging technique, the structure of the transported particles is clearly con-

firmed during and after the TAE burst. The highest detected energy of the transported particles is 150 keV, which is less than the injection beam energy of 180 keV. The energy slowing down time was 1.0–1.5 ms during the TAE burst, and 6–8 ms after the TAE burst. The energy slowing down during the TAE burst is considered to be related to the TAE burst frequency chirping down, and the energy slowing down after the TAE burst can be considered as the classical energy slowing down time.

[1] Cheng C. Z. and Chance M. S. 1986 Phys. Fluids **29**, 3695.
[2] Medley S. S. and Roquemore A. L. 1998 Rev. Sci. Instrum. **69**, 2651.
[3] Osakabe M. *et al.*, 2006 Nucl. Fusion **46**, S911-S917.
[4] Ogawa K. *et al.*, 2009 J. Plasma Fusion Res. SERIES **8**, 655.
[5] Ogawa K. *et al.*, 2010 Nucl. Fusion **50**, 084005.
[6] Fujiwara Y. *et al.*, 2020 JINST **15**, C02021.

(S. Kamio)

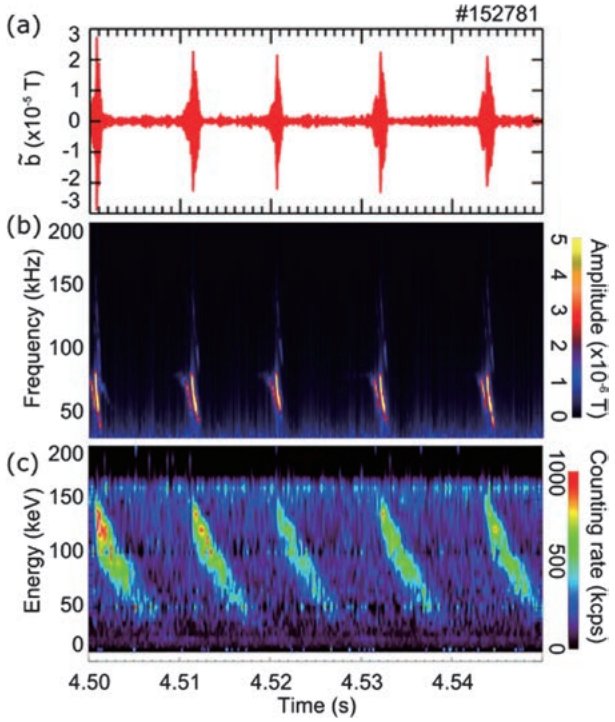

Fig. 4 Time evolutions of (a) the signal of the Mirov coil, (b) the spectrogram of the magnetic fluctuations, and (c) the energy spectrum of the particle flux Γ observed by E||B-NPA.

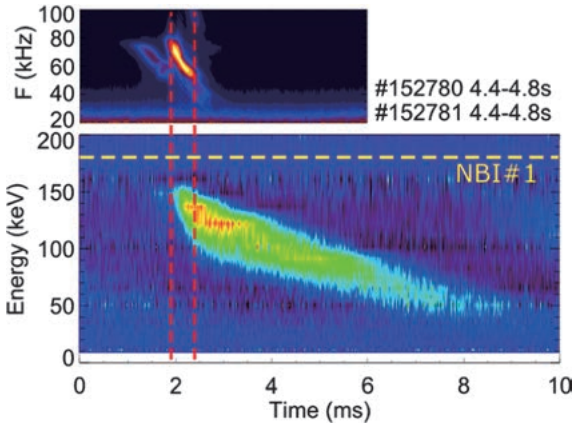

Fig. 5 The conditional averaged spectrogram of the magnetic fluctuation and the ΔΓ observed by E||B-NPA. Red dashed lines are the timing of the start and the end of the TAE bursts. Yellow dashed line is the injection energy of the NB #1.

Research and Development collaboration program for LHD-project

A special collaboration program, which is aimed to support the research and development activities in domestic universities for advanced diagnostics or heating scenarios, is established for future application on the LHD. One of the examples of such activity is shown in this section.

(M. Osakabe)

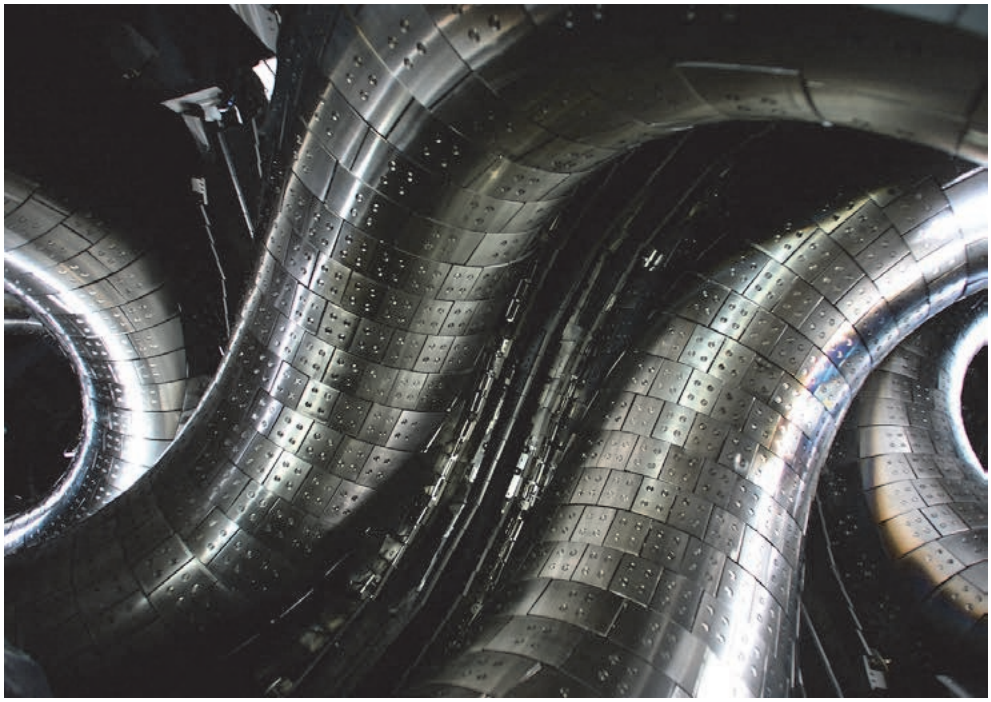

Figure. Inside the Large Helical Device

An RF induced transport model for the study of RF wave sustained plasmas

An RF transport model is constructed to understand the energy, momentum and particle confinement properties of lower hybrid wave sustained plasmas. Using the model, major properties of RF wave sustained TST-2 spherical tokamak plasmas are reproduced. The reproduction indicates that electrons are accelerated by the RF wave, and simultaneously transported toward a limiter and are lost.

Plasma current generation and sustainment by RF wave are important issues for spherical tokamak research. In most of the experiments so far, the obtained plasma density and the plasma current are relatively low. In such a case, RF induced transport of high energy electrons can be the dominant process determining the energy, momentum (i.e., current) and particle confinement of electrons. In the constructed model, the velocity evolution of an electron is obtained through the equation $\Delta V_{\parallel} = \widetilde{\Delta V}_{\parallel} - \nu_{\parallel} V_{\parallel} \Delta t - \frac{eE}{m} \Delta t$, where the terms in the RHS represent a random velocity change due to RF wave, collisional slowing down and acceleration by electric field, respectively. The orbit of an electron can be calculated from the velocity, and the electron is lost when the orbit touches one of the limiters. The electron velocity distribution function (EVDF) is obtained by following many electrons, and the plasma current, the deposited RF power, energy and particle confinement times are calculated from the EVDF. Some model parameters are adjusted to reproduce the measured plasma current, electron density and RF wave power. The model results suggest that major fraction of the deposited RF power, which generates fast electrons, is lost by the electrons hitting a limiter, while minor faction is used to heat bulk electrons and ions. From the energy distribution of the lost electrons, we can calculate the hard X-ray generation and the energy spectrum of measured hard X-rays. Figure 1 shows the calculated and the experimental hard X-ray spectra, and qualitative agreements between the experimental and the model results are shown.

[1] A. Ejiri *et al.*, Nuclear Fusion, being submitted.

(A. Ejiri, The University of Tokyo)

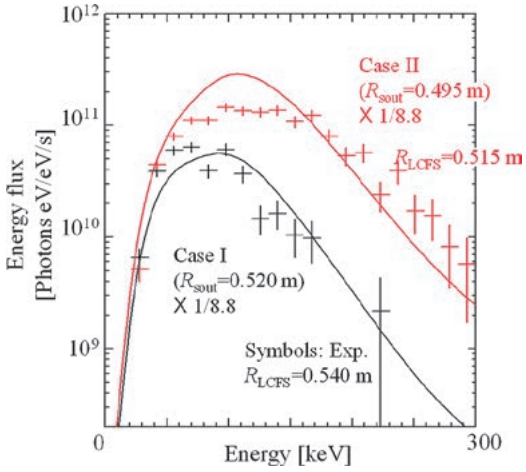

Fig. 1 Calculated (solid curve) and experimental (plus symbols) energy spectra. The calculated spectra are obtained by using the energy distribution of lost electrons in the model. They are multiplied by a factor of 1/8.8 in the plot to reproduce the experimental spectra. Two cases with different plasma sizes are shown by black and red.